Available online at www.sciencedirect.com

ScienceDirect

Advances in Space Research 72 (2023) 1224–1236

ADVANCES IN SPACE RESEARCH (a COSPAR publication)

www.elsevier.com/locate/asr

# On the low-latitude NeQuick topside ionosphere mismodelling: The role of parameters $H_0$, $g$, and $r$

M. Pezzopane [a,*], A. Pignalberi [a], B. Nava [b]

[a] Istituto Nazionale di Geofisica e Vulcanologia, Via di Vigna Murata 605, 00143 Rome, Italy
[b] The Abdus Salam International Centre for Theoretical Physics, Strada Costiera 11, 34151 Trieste, Italy

Received 11 November 2022; received in revised form 1 April 2023; accepted 7 April 2023
Available online 17 April 2023

**Abstract**

This paper deals with the well-known mismodelling characterizing the NeQuick topside ionosphere at low latitudes, i.e., the fact that the model keeps the two electron density humps typical of the equatorial ionization anomaly as the altitude increases from the height of the F2-layer electron density peak, without merging them in a single peak above the geomagnetic equator as expected. This is because the NeQuick topside ionosphere modelling strongly depends on several bottomside ionosphere parameters, which causes an essential coupling between the topside and the bottomside that in many cases behave differently. This means that this kind of topside ionosphere modelling may lead to inaccurate results, as it is the maintenance at low latitudes of the electron density double hump structure in the topside as the altitude increases. On the base of some recently published results, this paper analyzes the role played by the three NeQuick scale height parameters $H_0$, $g$ and $r$ in the description of the electron density above the F2 layer peak height. The results of this work pave the way for a possible solution of this low-latitude NeQuick topside ionosphere mismodelling.


*Keywords:* NeQuick model; IRI model; Low-latitude ionosphere; Topside ionosphere; COSMIC

## 1. Introduction

The topside ionosphere extends from the F2-layer peak height (*hm*F2) to the upper transition height (UTH), that is the height where the percentage of $O^+$ is equal to the percentage of light ions $H^+$ and $He^+$. The UTH exhibits very large variations as a function of location, local time, and solar activity level, ranging from about 500 km at night for low solar activity, to about 1600 km at daytime for high solar activity (Vaishnav et al., 2021). As a consequence, ionospheric models need to describe the electron density in a very large and varying spatial domain. In recent times, the ever growing importance of modern global navigation satellite system (GNSS) applications demands the knowledge of the electron density distribution also in the overlying plasmasphere, in order to obtain reliable total electron content values for GNSS signals correction (Hoque and Jakowski, 2012). This is why the most widespread empirical ionospheric models extend the modelling of the topside region well above the UTH, i.e., including the plasmasphere up to the altitude of the GNSS satellites at about 20,000 km. Then, although the UTH is historically considered as the top edge of the ionosphere, we here consider as topside also the lowest part of the overlying plasmasphere. Plasma transport processes and field-aligned plasma flows mainly set the plasma density distribution of this region (Rishbeth & Garriott, 1969), whose modelling is extremely important for telecommunication's purposes, because of the huge fraction of the total electron content it encloses

* Corresponding author.
*E-mail addresses:* michael.pezzopane@ingv.it (M. Pezzopane), alessio.pignalberi@ingv.it (A. Pignalberi), bnava@ictp.it (B. Nava).

https://doi.org/10.1016/j.asr.2023.04.014
0273-1177/

(Yizengaw et al., 2008; Habarulema et al., 2021; Park, 2022).

The modelling of the topside ionosphere is very challenging because it is hidden to the widely spread ground-based ionosonde measurements, and information on the electron density distribution at these altitudes can be obtained only through expensive techniques like topside sounders satellites, incoherent scatter radars, in-situ measurements by low-Earth-orbit (LEO) satellites, and radio occultation of GNSS signals (Hunsucker, 1991). The difficulties characterizing the modelling of the topside part of the ionosphere are testified by the fact that often the International Reference Ionosphere (IRI) model (Bilitza et al., 2022) does not represent properly its real features (Bilitza et al., 2006; Coïsson and Radicella, 2005; Coïsson et al., 2006; Pignalberi et al., 2016). For example, the first IRI topside formulation (Bilitza, 1990), the IRI2001, tended to overestimate the electron density and, in order to address this problem, Bilitza (2004) proposed a second option, the IRI2001-corr, by introducing a correction factor depending on the altitude, the modified dip latitude, and local time. Later on, to improve some shortcomings (Bilitza, 2009), a third IRI topside option, based on the NeQuick topside formulation (Nava et al., 2008; Coïsson et al., 2009; Radicella & Leitinger, 2001), was introduced and is still now the topside default option of the IRI model. Recently, Bilitza and Xiong (2021) proposed a fourth option based on in-situ measurements from CHAMP, GRACE, and Swarm satellites, as well as topside sounder data, to improve the IRI2001-corr option through the introduction of a solar activity correction factor.

It is worth highlighting that, besides the Epstein family functions (Rawer, 1988), as those used by NeQuick, other analytical functions were investigated in the past to represent the topside ionosphere. Among them, the Chapman (Chapman, 1931) and exponential functions, or a linear combination of these, were the most investigated. Several authors compared such functions against topside measurements to assess their suitability for the topside profile description. Fonda et al. (2005) compared α- and β-Chapman, and Epstein (with both constant and varying scale height) modelled topside profiles to those measured by topside sounders. In their comparison, α-Chapman profiles provided the best results, but emphasizing the need to improve the description of the topside shape far away from the F2-layer peak. Similarly, Verhulst and Stankov (2014) compared α- and β-Chapman, Epstein, and exponential topside profiles to topside sounders data. From their analysis, the exponential profile provided the best fit in almost 75 % of the analyzed cases, followed by α-Chapman. They also pointed out that the topside shape can be better described by a two-layer profile composed by an α-Chapman function for the lower part of the topside region and an exponential function for the upper part. Pignalberi et al. (2018a) calculated topside scale height values for the α- and β-Chapman, Epstein, and exponential functions by using in-situ electron density observations by European Space Agency Swarm satellites (Friis-Christensen, 2006, 2008). The comparison with radio occultation topside profiles measured by COSMIC/FORMOSAT-3 (hereafter COSMIC-1) (Anthes et al., 2008) highlighted that α-Chapman is the best function when using constant scale height values. However, the scale height exhibits a monotonic increasing trend in the topside ionosphere (Pignalberi et al., 2020a, 2020b) which has to be taken into account to get a reliable description of the topside shape at different altitude ranges. This is what is done in the vary-Chapman approach (Reinisch et al., 2007; Nsumei et al., 2012; Prol et al., 2022), and in the Epstein approach with variable scale height as in NeQuick (Nava et al., 2008; Pignalberi et al., 2020a, 2020b) and in the Empirical-Canadian High Arctic Ionospheric Model (E-CHAIM; Themens et al., 2018). These works show that, to perform a reliable description of the topside, rather than by a specific analytical function, the major role is played by a faithful description of the scale height vertical variation. A reliable modelling of the topside scale height vertical variation makes it possible to describe the change in the shape of the topside profile from the $O^+$ dominated ionosphere just above the F2-layer peak to the $H^+$ dominated plasmasphere. This is the rationale behind the NeQuick topside scale height formulation and later developments, including this paper. It is worth highlighting that the empirical scale height values used for topside ionosphere empirical modelling usually differ from theoretical scale height values derived from the plasma ambipolar diffusion theory (Pignalberi et al., 2020b). In fact, empirical scale height values are derived directly from electron density observations; then, they are effective in reproducing the observed electron density topside profile with the assumed analytical parameterization. Differently, theoretical scale height values are derived from the knowledge of the ionospheric plasma physical state and chemical composition in the framework of the plasma ambipolar diffusion theory. Pignalberi et al. (2020b) showed how empirical effective scale height values and theoretical scale height values differ in magnitude at the F2-layer peak and in the lower topside. However, they tend towards each other in the upper topside, by reaching similar values within a few hundreds of kilometers above the F2-layer peak.

This paper focuses on the NeQuick topside modelling and specifically on its low-latitude mismodelling which consists in keeping the two electron density humps typical of the equatorial ionization anomaly (EIA) as the altitude increases from *hm*F2, without merging them in a single peak above the geomagnetic equator as expected. This fact was highlighted for the first time by Bilitza (2009) and recently remarked by Kashcheyev and Nava (2019) and by Bilitza and Xiong (2021). In particular, Kashcheyev and Nava (2019) thoroughly investigated the ability of the NeQuick topside model in representing the total electron content (TEC) in the topside ionosphere – plasmasphere system in the height range between about 800 km and 20,000 km. They compared NeQuick modelled TEC

values with corresponding values measured by precise orbit determination (POD) antennas onboard COSMIC-1 in the period 2006–2018. Their comparison showed that NeQuick underestimates the TEC in the topside ionosphere – plasmasphere system on average by −3.73 TECU (1 TECU = $10^{16}$ el/cm$^2$), ranging between −2 and −8 TECU depending on location, local time, season, and solar activity. Moreover, they found that NeQuick modelled TEC values show two maxima located above the EIA, while POD measured data show a single broad peak around the geomagnetic equator. The impact of this electron density mismodelling by NeQuick is particularly evident when focusing on very high altitudes but it has a minor effect when considering TEC values for the entire ionosphere – plasmaphere system as recorded by ground-based GNSS receivers.

Here we want to underline the fact that, exploiting the results of two recently published works (Pignalberi et al., 2020a, 2022), the aim of the work is mainly to show a possible way to solve this NeQuick topside mismodelling. To support this, a small validation analysis based on data recorded by different LEO satellite missions will be also shown.

Section 2 represents a recall of both the NeQuick topside modelling and the main results obtained by Pignalberi et al. (2020a, 2022). Section 3 will describe the methodology used to smooth out the low-latitude NeQuick topside mismodelling and discuss the corresponding results. Section 4 will describe a validation analysis based on LEO satellites. The summary and conclusions will be the subject of Section 5.

## 2. The NeQuick topside representation and some recent studies on it

The NeQuick topside modelling approach started with Leitinger et al. (2001, 2002) and Radicella and Leitinger (2001) and evolved from its original formulation to the current version (Nava et al., 2008; Coïsson et al., 2006), which consists of a semi-Epstein layer describing the topside electron density $N_e$ as a function of the height $h$, starting from the F2-layer electron density maximum $NmF2$ at the $hmF2$ height

$$N_e(h) = 4NmF2\frac{\exp\left(\frac{h-hmF2}{H}\right)}{\left[1+\exp\left(\frac{h-hmF2}{H}\right)\right]^2} \quad (1)$$

where $H$ is a height-dependent scale height

$$H(h) = H_0\left[1+\frac{r\cdot g\cdot(h-hmF2)}{r\cdot H_0+g\cdot(h-hmF2)}\right] \quad (2)$$

with $r$ and $g$ which are constant factors equal to 100 and 0.125, respectively. $H_0$ is instead the value of $H$ at the F2-peak height $hmF2$ and equal to

$$H_0 = k\cdot B_{2bot} \quad (3)$$

where $B_{2bot}$ is the NeQuick bottomside thickness parameter (Leitinger et al., 2005; Radicella et al., 2021), which represents the scale height of the F2-layer bottomside region; $k$ is defined as

$$k = 3.22 - 0.0538foF2 - 0.00664hmF2 + 0.113\frac{hmF2}{B_{2\,bot}} + 0.00257R_{12} \quad (4)$$

with $R_{12}$ the 12-month running-mean of the sunspot number $R$ and $foF2$ the critical frequency of the ordinary mode of propagation associated to $NmF2$; $B_{2bot}$ is linked to the density derivative at the inflection point $(dN_e/dh)_{max}$ of the semi-Epstein layer representing the bottomside F2 layer in the following way

$$B_{2bot} = \frac{0.04774foF2^2}{\left(\frac{dN_e}{dh}\right)_{max}} \quad (5)$$

Mosert de Gonzales and Radicella (1990) using ionosonde data found the following empirical relationship for $(dN_e/dh)_{max}$

$$\left(\frac{dN_e}{dh}\right)_{max} = 0.01 \times \exp\left[-3.467+1.714\ln(foF2)+2.02\ln(M(3000)F2)\right] \quad (6)$$

where $M(3000)F2$ is the F2-layer propagation factor for a distance of 3000 km.

Looking at relationships (2)-(6), it is clear how the NeQuick topside modelling significantly depends on the F2-layer and bottomside parameters ($hmF2$, $NmF2$, $foF2$, $M(3000)F2$), which causes an important coupling between the topside and the bottomside scale height. This way to model the topside region allows a smooth transition between the bottomside and the topside regions, which is critical for ray-tracing and tomographic applications. However, it may lead to incorrect results, as it is the preservation at low latitudes of the electron density double hump structure in the topside as the altitude increases.

Recently, Pezzopane and Pignalberi (2019) inferred a new representation of $H_0$, that they called $H_{0,corr}$, by forcing the NeQuick topside formulation (1) to join the F2-layer peak characteristics ($hmF2$ and $NmF2$), as provided by the IRI UP method over the European region (Pignalberi et al., 2018b, 2018c), and the in-situ electron density value as measured by Langmuir probes on board Swarm satellites (Friis-Christensen, 2006, 2008). However, this approach, also strongly dependent on the F2-layer parameters, even though it improves the topside description made by the NeQuick model, especially at mid latitudes for both high and low solar activities, it cannot merge the two humps of the equatorial ionization anomaly as the altitude increases.

Pignalberi et al. (2020a) studied the NeQuick topside scale height given by Eq. (2) just above the F2-layer peak by expanding it in a Taylor series around $hmF2$, and they

pointed out that at the first-order of approximation it shows a linear dependence on the reduced height *h*-*hm*F2

$$H(h) \simeq H_0 + g \cdot (h - hm\mathrm{F2}) \tag{7}$$

with $H_0$ representing the intercept and $g$ the slope (namely the vertical gradient of the scale height above *hm*F2); a result that is coherent with the interpretation of Themens et al. (2018) and that was firstly investigated by Nava et al. (2001) through INTERCOSMOS-19 topside sounders data. Pignalberi et al. (2020a) also pointed out that, as the height approaches infinity, the NeQuick topside scale height can be approximated to

$$H \simeq H_0 \cdot (1 + r) \tag{8}$$

Equation (8) clearly shows how the parameter $r$ of the NeQuick topside formulation controls the asymptotic behavior of the scale height, i.e., the electron density distribution at plasmaspheric altitudes (Leitinger et al., 2002).

Pignalberi et al. (2020a) described also a method to obtain the effective topside scale height $H(h)$ by analytically inverting Eq. (1), and obtained the following expression

$$H(h) = \frac{h - hm\mathrm{F2}}{\ln\left\{\frac{1}{N_e(h)}\left[(2Nm\mathrm{F2} - N_e(h)) + 2\sqrt{Nm\mathrm{F2}^2 - N_e(h) \cdot Nm\mathrm{F2}}\right]\right\}} \tag{9}$$

Equation (9) allows getting scale height values once $N_e(h)$, *Nm*F2, and *hm*F2 measurements are available. This method was first considered by Pignalberi et al. (2020a) with a small selected COSMIC-1 dataset of radio occultation (RO) topside electron density profiles and then by Pignalberi et al. (2020b), who considered the whole COSMIC-1 dataset.

Using Eq. (9), and exploiting a selected dataset of about 1.8 millions of COSMIC-1 RO topside electron density profiles, Pignalberi et al. (2022) globally retrieved for the first time the NeQuick topside parameters $H_0$, $g$, and $r$ on a global basis and for different conditions. Their results show that these parameters are affected by large spatial, diurnal, and seasonal variations and by an important dependence on both solar and magnetic activities, while before that study the NeQuick $g$ and $r$ parameters were considered constant. The datasets they found are very valuable, particularly those of $H_0$ and $g$. Concerning $r$, they noted that its increasing trend from high to low latitudes suddenly stopped at about ± 30° of magnetic latitude by reaching values close to zero. Investigating this peculiar behavior, they understood that the magnitude decrease of $r$ at low latitudes is a consequence of the limited COSMIC-1 satellites orbit altitude, which is at most 800 km. In fact, in general, low-latitude electron density profiles are characterized by *hm*F2 values much higher than those at other latitudes, and in these cases the topside altitudinal extension of the RO profiles retrieved by COSMIC-1 is significantly reduced. Given that the $r$ parameter drives the scale height variation at heights significantly larger than *hm*F2, it is not possible to estimate its value from topside profiles that are so little extended in height. They concluded that the $r$ behavior between ± 30° of magnetic latitude almost certainly is an artifact and cannot be considered as real.

The next section will show how these results turn out to be valuable to face the low-latitude NeQuick topside mismodelling, which is the subject of this work.

## 3. The low-latitude NeQuick topside mismodelling: Discussion on some tests to mitigate the problem

Bilitza (2009) was the first who highlighted the low-latitude NeQuick topside mismodelling consisting in keeping the two electron density humps typical of the EIA as the altitude increases from *hm*F2. With regard to this, Fig. 1 reports a revised form of the plots shown by Bilitza (2009) in his Fig. 5, valid for the following conditions: meridian at longitude 0°, 16:00 universal time, Northern summer season, medium solar activity ($R_{12} = 50$).

The figure shows that the IRI2001 model produces unrealistic, almost constant with altitude, profiles in the upper topside, while the IRI2001-corr model well merges the double structure as the altitude increases. Instead, the NeQuick model, which is the default option of the IRI model, keeps the double structure typical of the EIA as the altitude increases.

Our analysis will be based on Fig. 1c, the one related to the NeQuick model. In detail, based on the results found by Pignalberi et al. (2020a, 2022), we will generate several NeQuick plots, each of which characterized by different values of the three NeQuick topside parameters $H_0$, $g$, and $r$. This is done with the aim to find whether there is a specific combination of the three parameters that succeeds in fixing the low-latitude NeQuick mismodelling.

Fig. 2 reports the three NeQuick topside parameters retrieved through COSMIC-1 RO electron density profiles according to Pignalberi et al. (2022), in geomagnetic latitude versus local time. Differently from the plots shown in Pignalberi et al. (2022), to generate those in Fig. 2 we applied first a two-dimensional Gaussian kernel filter and subsequently a bivariate spline approximation over a rectangular mesh filter. This allows getting for each of the three parameters meridional curves, which are the ones we are interested in, that are as much continuous and smooth as possible. It should be noted here that in Fig. 2 the longitudinal dependence is lost.

Fig. 3a–c shows the meridional profiles of $H_0$, $g$, and $r$, corresponding to 16:00 local time, that is the time considered to generate the plots shown in Fig. 1 (since the meridian at longitude 0° has been considered), as extrapolated from Fig. 2 (those corresponding to the dashed black vertical lines). These meridional profiles are then used to generate a latitudinal electron density NeQuick plot at longitude 0° (see Fig. 3d), as the one shown in Fig. 1c.

It is important here to highlight that, while the latitudinal plots of Fig. 1 refer to both a well-defined season (sum-

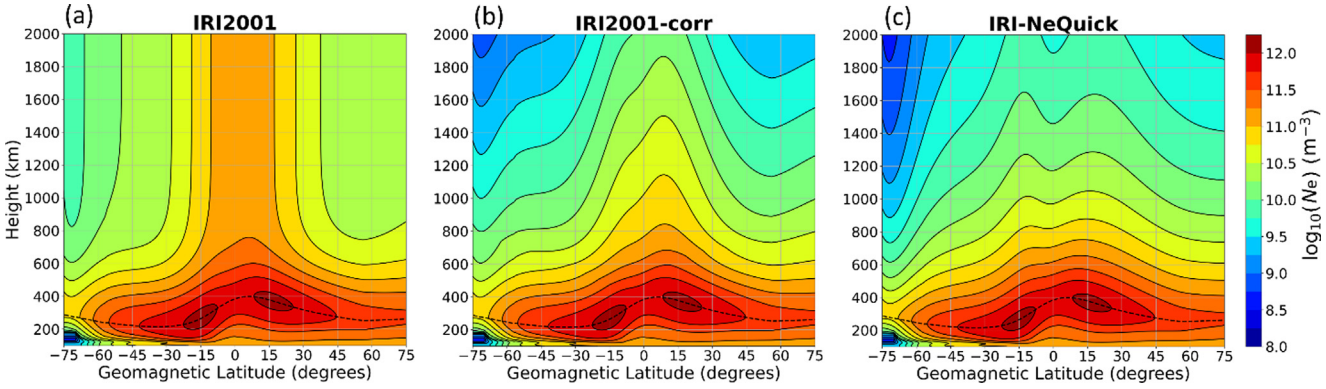


Fig. 1. Geomagnetic latitude versus height plots of the logarithm of the electron density at longitude 0° and universal time 16:00 in Northern summer season, for medium solar activity ($R_{12} = 50$), for (a) IRI2001, (b) IRI2001-corr, and (c) NeQuick, for the altitude range 100–2000 km. The dotted black curve in each plot represents the altitude of the absolute maximum of electron density.

mer in the Northern hemisphere) and solar activity ($R_{12} = 50$), the values of $H_0$, $g$, and $r$ shown in Fig. 2 have been instead generated including all seasons and solar activities, as in Pignalberi et al. (2022). Restricting the analysis of Fig. 2 to the Northern summer season and to a well-defined solar activity would have meant to reduce drastically the amount of available COSMIC-1 RO profiles, thus making impossible to generate plots statistically significant. We are aware of this limitation of the analysis and some consequences of this choice will be clarified later. Moreover, we want to remark again here that Fig. 2 does not consider the longitudinal dependence of the three topside parameters.

Fig. 3d shows that at low latitudes the very low values (almost null) of $r$ cause a too fast decrease of the electron density, due to a too small scale height. On the other hand, the single equatorial peak is well reproduced, even though instead of having an absolute maximum the sudden decrease of $r$ causes a plasma hole. However, it is promising the fact that $H_0$ and $g$ retrieved from COSMIC-1 can reproduce the single equatorial peak even without $r$, which is practically null in that region.

In virtue of this result, we made an additional test, namely to generate other latitudinal electron density NeQuick plots at longitude 0°, considering for $H_0$ and $g$ the latitudinal profiles shown in Fig. 3a-b and for $r$ constant values respectively equal to 0, 15, and 100. $r = 100$ is the value usually considered by the NeQuick model to represent the topside. Instead, $r = 15$ is a value that derives from purely theoretical considerations under diffusive equilibrium conditions (Leitinger et al., 2002); specifically, as a first approximation, $H$ scales by a factor of 16 going from *hm*F2 (where $H = H_0$) to infinity where Eq. (8) holds, because we move from a region dominated by $O^+$ to a region dominated by $H^+$, and to take this into account $r$ must be equal to 15. It is worth highlighting that this is a very coarse approximation which does not consider the vertical variation of the acceleration of gravity and of the plasma temperature, which both play an important role in the plasma scale height calculation (Pignalberi et al., 2020b).

Fig. 4 shows the corresponding results.

Setting $r = 0$, which means to eliminate also the contribution of the parameter $g$ (see Eq. (2)), corresponds to fix $H = H_0$ along the whole topside profile. This is useful to evaluate how $H_0$ affects the topside, and Fig. 4c shows that $H_0$ alone can generate a single equatorial peak as the altitude increases, even though $H_0$ is the scale height at *hm*F2, that is an altitude characterized by the double structure. The price to pay of course is that the electron density decreases too fast with the altitude, due to a scale height constant throughout the entire topside profile. Anyhow, the shape of the meridional profile at low latitudes matches that obtained from independent observations (Kashcheyev and Nava, 2019; He et al., 2022).

The tests with $r = 15$ and $r = 100$ instead show that the values of $g$ and $r$ retrieved through COSMIC-1 must be used simultaneously. This is because COSMIC-1 RO electron density profiles used by Pignalberi et al. (2022) to perform the non-linear fit of the scale height (9) do not reach infinity (they stop at most at about 800 km, which is the maximum COSMIC-1 orbit altitude), so it is not possible to decouple the contribution of $r$ and $g$ to the scale height. To make a correct estimate of $r$ and $g$, there would be a need for electron density profiles that reach much larger altitudes where the effect of $r$ is much greater than that of $g$. This is the reason behind the bad results of Fig. 4a-b with $r = 100$ and $r = 15$, where we used the $g$ values obtained through COSMIC-1 but we fixed an a-posteriori value for $r$.

According to the aforementioned results, an additional test we made was to consider for $H_0$ the latitudinal profile shown in Fig. 3a and for $g$ and $r$ constant values. The couple of values considered for $g$ and $r$ are: $g = 0.125$ and $r = 100$, that are the constant values usually considered by the NeQuick topside modelling; $g = 0.2024$ and $r = 20$, that are the constant values found by Themens et al. (2018) for Northern middle-high latitudes;

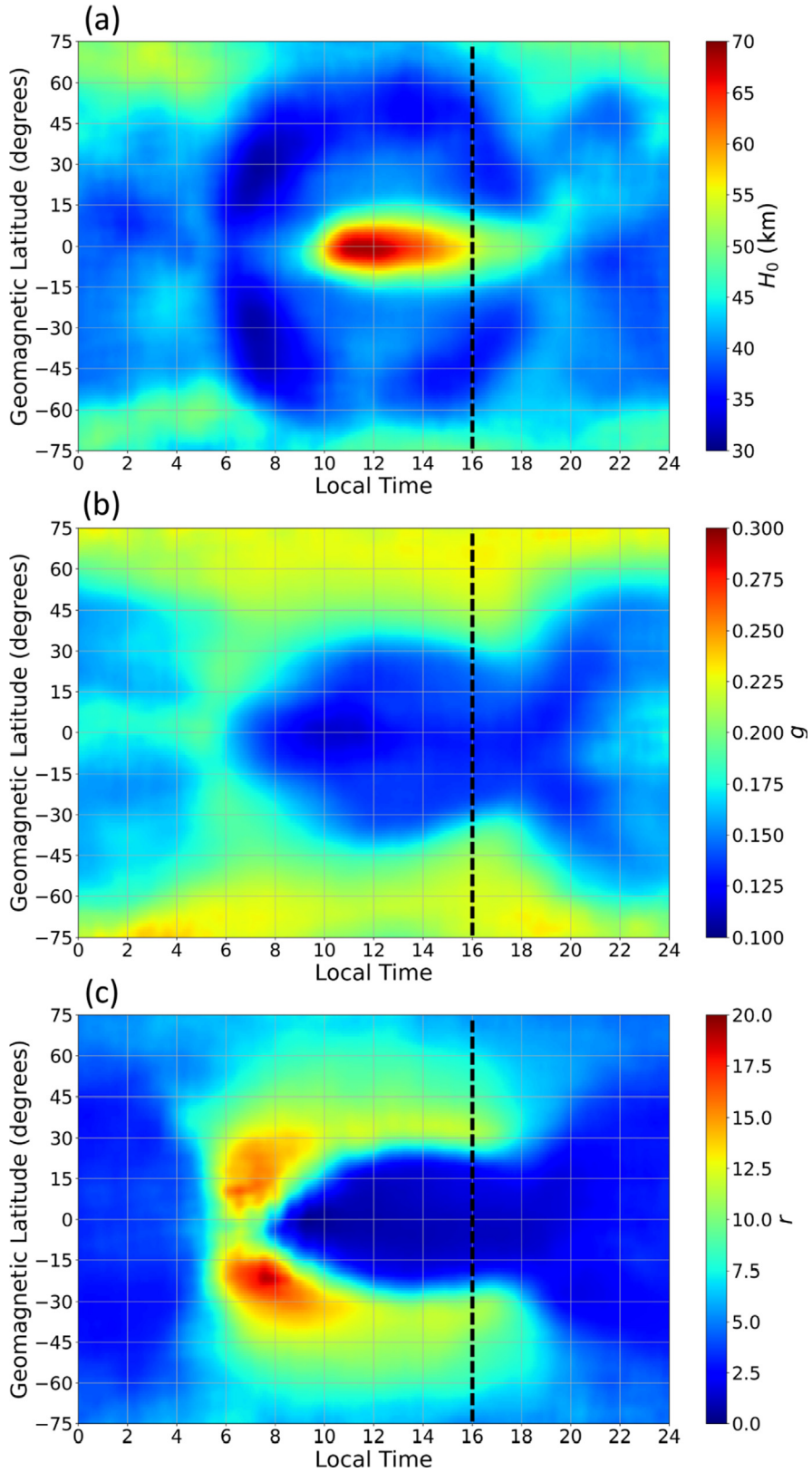


Fig. 2. NeQuick topside parameters (a) $H_0$, (b) $g$, and (c) $r$, retrieved through COSMIC-1 RO electron density profiles according to Pignalberi et al. (2022), and plotted in geomagnetic latitude versus local time. The dashed black vertical line in each plot highlights the values corresponding to 16:00 local time, which is the time considered by Bilitza (2009) to generate the plots shown in Fig. 1.

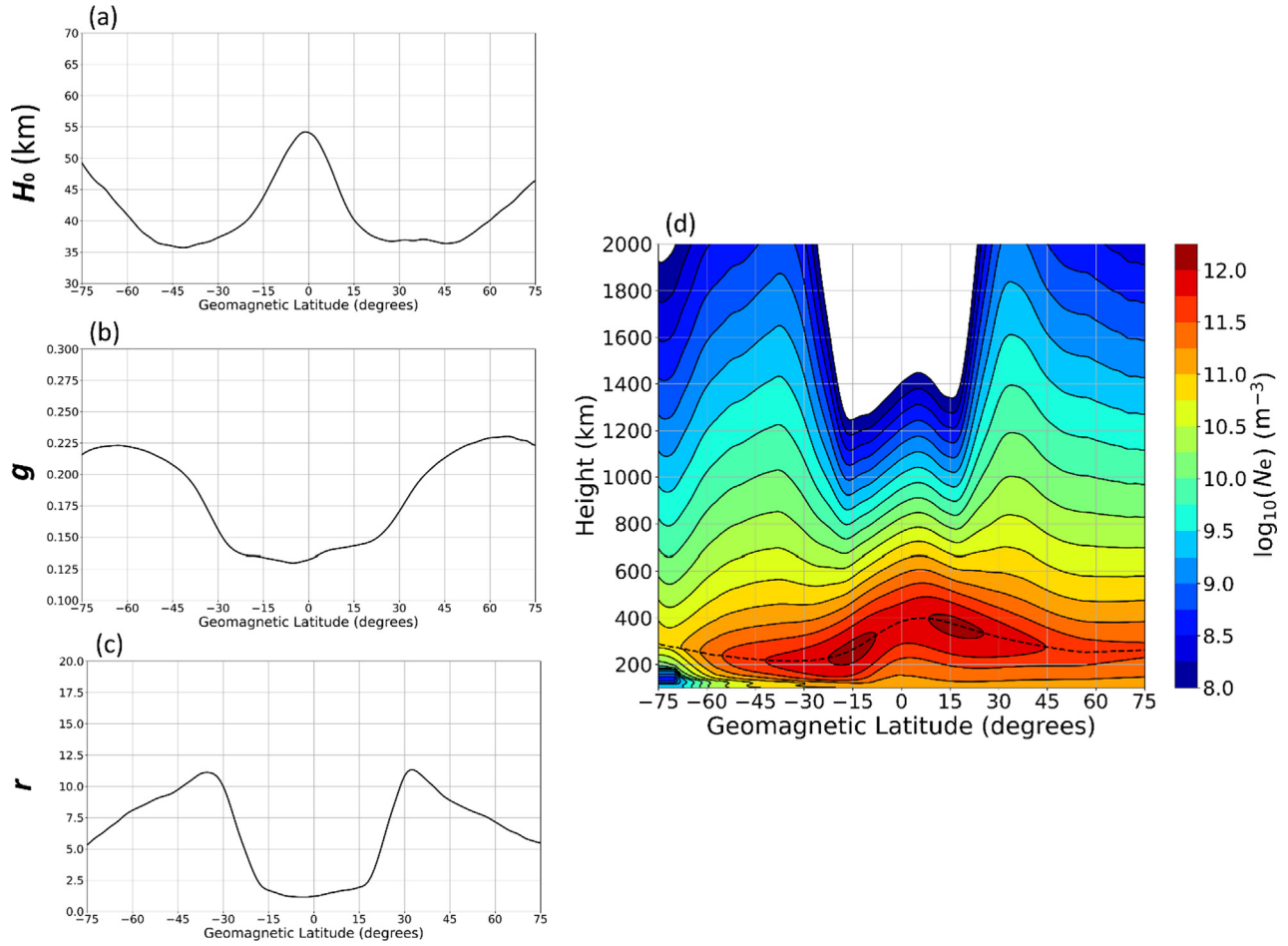


Fig. 3. Meridional profiles of (a) $H_0$, (b) $g$ and (c) $r$, corresponding to 16:00 local time, that is the time considered to generate the plots shown in Fig. 1, as extrapolated from Fig. 2. (d) The latitudinal electron density NeQuick plot at longitude 0° generated using the meridional profiles of $H_0$, $g$, and $r$ shown in (a-c). The dotted black curve represents the altitude of the absolute maximum of electron density.

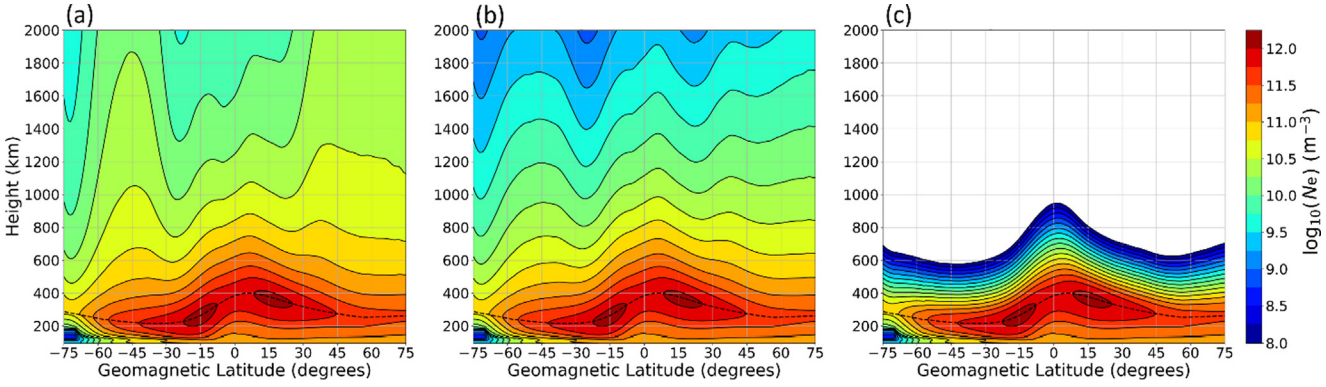


Fig. 4. Latitudinal electron density NeQuick plots at longitude 0° generated using the meridional profiles of $H_0$ and $g$ shown in Fig. 3a-b and $r$ constant values respectively equal to (a) 100, (b) 15 and (c) 0. The dotted black curve in each plot represents the altitude of the absolute maximum of electron density.

$g = 0.188$ and $r = 15$, where the value for $g$ corresponds to the average over the meridional profile shown in Fig. 3b.

Fig. 5 displays the corresponding results and shows that in this case, when compared to Fig. 4, the results are by far better.

This confirms that $H_0$, to be more precise its variation with latitude, is a powerful parameter that can well reproduce the single crest as the altitude increases from *hm*F2. Fig. 5a-b are both characterized by a small minimum over the geomagnetic equator and by a different electron density

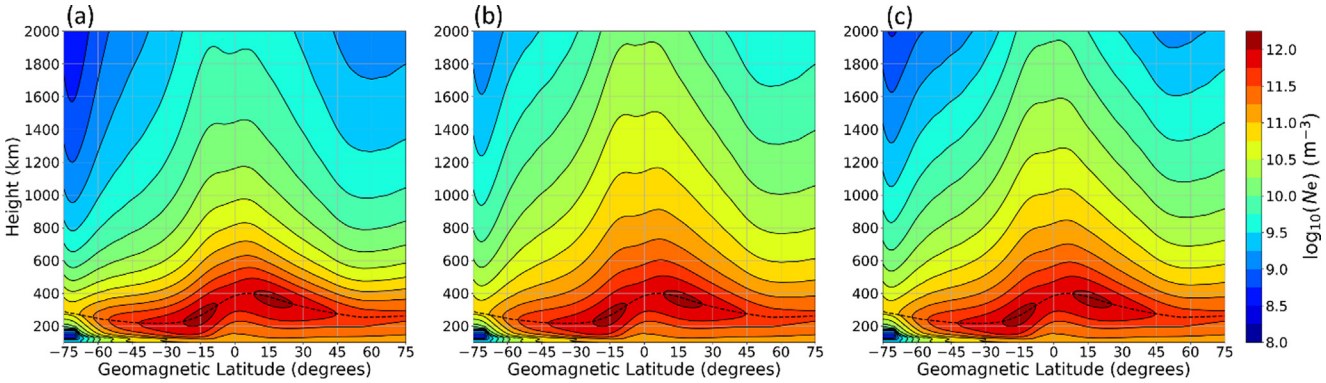


Fig. 5. Latitudinal electron density NeQuick plots at longitude 0° generated using the meridional profile of $H_0$ shown in Fig. 3a and for $g$ and $r$ the following constant values: (a) $g = 0.125$ and $r = 100$; (b) $g = 0.2024$ and $r = 20$; (c) $g = 0.188$ and $r = 15$. The dotted black curve in each plot represents the altitude of the absolute maximum of electron density.

gradient with the altitude, larger in Fig. 5a and smaller in Fig. 5b, according to the different $g$ values. Instead, Fig. 5c shows that considering $g = 0.188$ and $r = 15$ allows obtaining a single crest over the geomagnetic equator and regular structures at middle and high latitudes, with an electron density gradient with the altitude which is reasonable and comparable with that of Fig. 1b.

It is worth highlighting here that similar results to those displayed in Figs. 4-5 have been obtained also applying the methodology proposed by Pignalberi et al. (2020b), i.e., considering only the altitude range where the scale height shows a linear dependence on the height according to Eq. (7). Of course, in this case the plots as those shown in Fig. 2 are obtained only for $H_0$ and $g$. It is in fact well demonstrated that the topside scale height exhibits a linear dependence on height until an altitude of about 800 km (Olivares-Pulido et al., 2016; Prol et al., 2018, 2019, 2022; Pignalberi et al., 2020a, 2020b; Singh et al., 2021). Therefore, a model taking into account only the parameters $H_0$ and $g$ would provide a faithful representation of the topside ionosphere up to about 800 km of altitude. Anyhow, since we are here interested in describing the full topside profile, up to GNSS satellites altitudes, the inclusion of the $r$ parameter in the NeQuick topside scale height of Eq. (2) is essential to restrict the scale height increase at very high altitudes.

## 4. Comparison with electron density observations by LEO satellites

To validate the results described in Section 3, we compared the modelled electron density latitudinal profiles with the ones obtained through LEO satellites measurements, for different altitudes in the topside ionosphere. To achieve this result, we selected in-situ electron density observations made by several LEO satellites for the same local time, season, and solar activity conditions studied in Section 3. It is important to highlight here that the results obtained by Bilitza (2009), as reproduced in Fig. 1, were obtained by selecting $R_{12} = 50$. Anyway, since then the sunspot number calculation method has changed (Clette et al., 2014; Clette and Lefèvre, 2016; Cliver 2016). The $R_{12} = 50$ value used by Bilitza (2009) refers to the old version of the sunspot number, which is used in several IRI sub-models as solar activity proxy (Bilitza et al., 2022). Therefore, to select LEO satellites observations for a similar solar activity level, we first needed to calculate the value corresponding to the new sunspot number formulation. Currently, IRI model applies a constant conversion factor to obtain the old sunspot number ($R_{old}$) given the new one ($R_{new}$); specifically, $R_{old} = 0.7 \cdot R_{new}$. We used a little more refined conversion procedure between $R_{new}$ and $R_{old}$ as derived by Pignalberi et al. (2021) based on data from 1964 to 2015

$$R_{new} = 1.401 \cdot R_{old} + 1.030 \quad (10)$$

By applying Eq. (10) we obtained $R_{new} \approx 71$ when $R_{old} = 50$. Therefore, we selected LEO satellites observations recorded with a solar activity level around $R_{new} \approx 71$, for Northern summer season, and at 16:00 ± 01:00 local time.

For our comparison, we used electron density observations as recorded by the following LEO satellites: CHAllenging Minisatellite Payload (CHAMP) planar Langmuir Probe (LP) data at about 385 km of altitude for June and July 2004 (Reigber et al., 2004; Rother and Michaelis, 2019); Swarm A spherical LP data at about 460 km of altitude for May, June, July, and August 2022 (Knudsen et al., 2017; Catapano et al., 2022); Swarm B spherical LP data at about 515 km of altitude for May, June, July, and August 2022; Ionospheric Connection Explorer (ICON) ion velocity meter data at about 590 km of altitude for June 2022 (Immel et al., 2018; Heelis et al., 2017); Defense Meteorological Satellite Program (DMSP) F15 Special Sensors-Ions, Electrons, and Scintillation (SSIES) data at about 850 km of altitude for May, June, July, and August 2012 (Garner et al., 2010). CHAMP data were downloaded from ftp://isdcftp.gfz-potsdam.de/champ/ME/Level2/PLPT/, Swarm A and B data from ftp://swarm-diss.eo.esa.int/Level1b/Latest_baselines/EFIx_LP/, ICON data from ftp://icon-science.ssl.berkeley.edu/pub/LEVEL.2/IVM-A, and DMSP F15 data

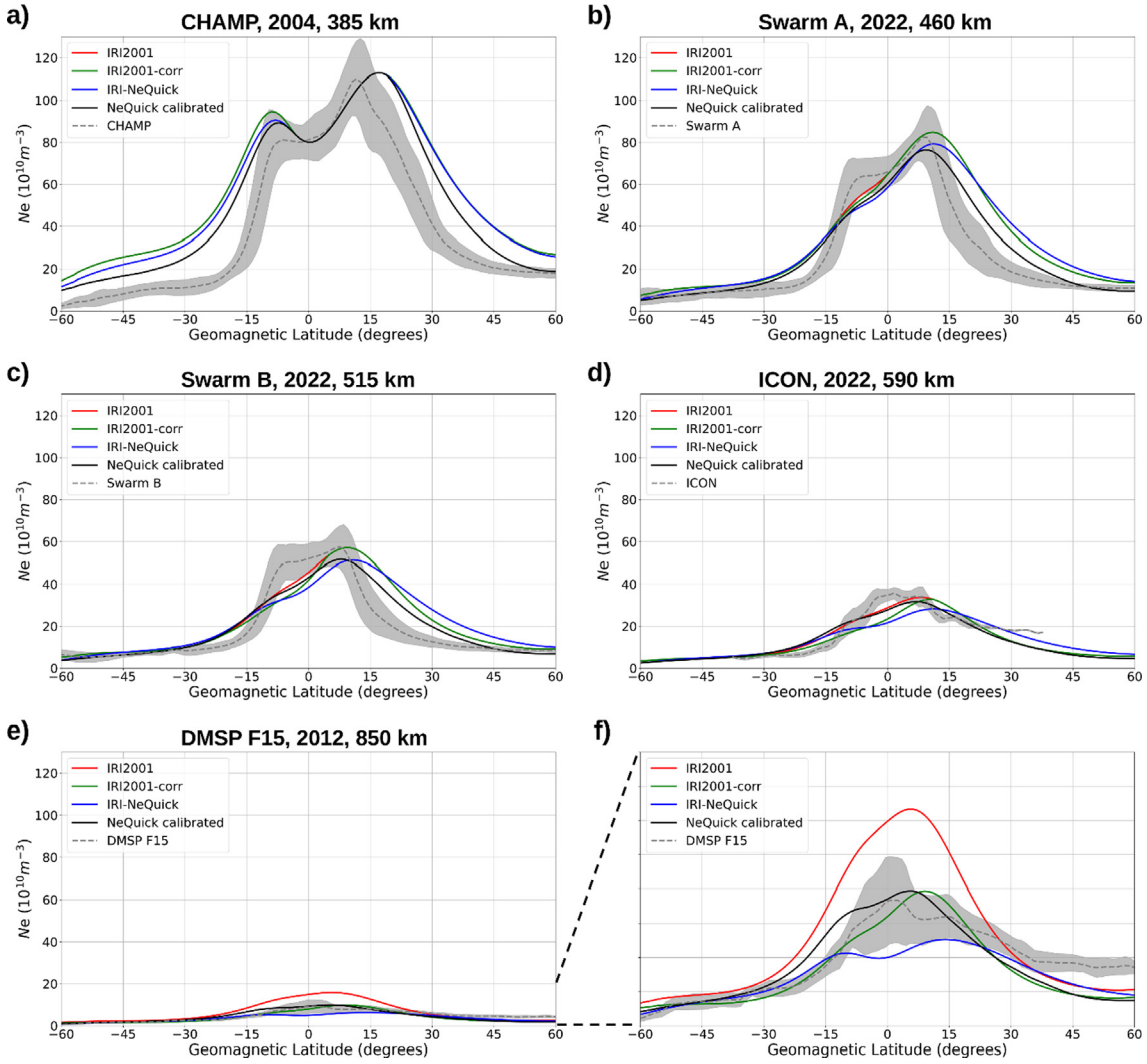


Fig. 6. Latitudinal electron density profiles calculated according to the modelled latitudinal electron density profiles shown in Fig. 1a–c (IRI2001 in red, IRI2001-corr in green, and IRI-NeQuick in blue, respectively) and Fig. 5c (Nequick calibrated in black), and as measured by different LEO satellites (dashed grey curve is the mean value, shadow grey area represents the dispersion in terms of two standard deviations), for different altitudes. Panel a) shows values at 385 km of altitude with observations by CHAMP in 2004. Panel b) shows values at 460 km of altitude with observations by Swarm A in 2022. Panel c) shows values at 515 km of altitude with observations by Swarm B in 2022. Panel d) shows values at 590 km of altitude with observations by ICON in 2022. Panel e) shows values at 850 km of altitude with observations by DMSP F15 in 2012. Panel f) is a zoom of panel e). All plots refer to the 16:00 ± 01:00 local time and Northern summer conditions for medium solar activity.

from the CEDAR Madrigal database at http://cedar.openmadrigal.org/.

Fig. 6 shows the latitudinal electron density profiles as modelled by the three IRI topside options of Fig. 1a–c, and as given by NeQuick with calibrated topside parameters of Fig. 5c, compared with those obtained through LEO satellites observations at different altitudes. Measured electron density data are represented in grey, where the dashed curve is the mean value with the shadow grey area representing the statistical dispersion in terms of two standard deviations.

In Fig. 6, the use of LEO satellites data at different altitudes allows investigating the latitudinal behavior of the electron density as the height above the F2-layer peak increases. Differences between modelled and measured data could arise due to an incorrect description of both the modelled topside profile shape, and the modelled F2-layer peak anchor point (both *hm*F2 and *Nm*F2). Since the F2-layer peak parameters are not available from these LEO satellites, it has not been possible to eliminate the possible error related to the F2-layer peak description by feeding the models with measured *hm*F2 and *Nm*F2 values. Aware of this limitation, we focus mainly on the latitudinal variations, at different altitudes, shown by data and models, giving less importance to absolute differences between them. By considering the latitudinal variation at low latitudes, observations by LEO satellites show how the electron density exhibits the double crest structure

of the EIA at CHAMP altitude, which is very close to *hm*F2 at low latitudes (see the dotted black curve of Fig. 1 for reference). By increasing the altitude and going deep in the topside, the double crest structure gradually disappears, as shown by Swarm A and B panels, and then a single broad maximum around the magnetic equator appears already at ICON altitude, and becomes clearer at DMSP F15 altitude. Observations at lower altitudes (panels a, b, and c of Fig. 6) show a hemispheric asymmetry characterizing the electron density maxima values of EIA humps, with the Northern hump higher than the Southern one. This is because we are considering the Northern hemisphere summer season. This hemispheric difference gradually disappears at higher altitudes (panels d, e, and f of Fig. 6). Differently, hemispheric differences at mid and high latitudes, with the highest values in the summer hemisphere, persist also at higher altitudes. Modelled values do not succeed in catching all the latitudinal and altitudinal variations shown by measured data, and differences between the modelled values are evident. At CHAMP altitude, modelled values are very similar each other being very close to *hm*F2. They correctly describe the double crest structure with corresponding hemispheric differences due to the season, but the location of the two maxima and the transition to mid latitudes can be improved. At higher altitudes, differences among the modelled values are more evident in both shape and magnitude. In general, the oldest IRI2001 option exhibits the well-known overestimation at low latitudes; such behavior was fixed by the introduction of the IRI2001-corr option. Both of these IRI options succeed in describing the main latitudinal variation at different altitudes, but, at higher altitudes, they tend to keep the single maximum shifted to Northern latitudes instead of representing it above the geomagnetic equator. The IRI-NeQuick option shows a double crest structure at all altitudes with underestimated values at low latitudes. The use of calibrated values of $H_0$, $g$, and $r$ parameters allows improving the NeQuick topside description in both the latitudinal variation and the magnitude. The smooth altitudinal transition between double and single maxima at low latitudes is partly described by NeQuick calibrated profile, with values that are compatible in magnitude with those observed. It is worth reminding that calibrated values of $H_0$, $g$, and $r$ used to obtain NeQuick calibrated values (black curves in Fig. 6) were obtained without a seasonal sorting. This is why $H_0$, $g$, and $r$ values are symmetric with respect to the geomagnetic equator (see Fig. 2 and Fig. 3). Moreover, no solar activity partitioning was applied to obtain $H_0$, $g$, and $r$ values shown in Fig. 2 and Fig. 3. These are all issues that need to be faced in the future, as highlighted by Pignalberi et al. (2022). However, Fig. 6 shows how the NeQuick topside model can accurately describe the electron density latitudinal and altitudinal variations with a proper choice and modelling of the three topside parameters used for the topside scale height description.

## 5. Summary and conclusions

This paper focuses on a specific shortcoming shown by the NeQuick model when representing the topside ionosphere at low latitudes, namely the fact that it keeps the typical double structure of the EIA anomaly as the altitude increases from the height *hm*F2 of the F2-layer peak.

Based on some recent results that have been obtained using COSMIC-1 RO data, we performed some tests with a dual purpose: a) to mitigate this low-latitude NeQuick mismodelling; b) to understand what is the specific role played by each of the three topside parameters $H_0$, $g$, and $r$ considered by the NeQuick model to represent the topside ionosphere.

The results of this study show that there exist suitable combinations of the three topside parameters that properly face this issue, which allows the NeQuick model to describe the expected latitudinal variation of the electron density in the topside ionosphere when compared to in-situ observations by LEO satellites at different altitudes. This result represents a novelty because it demonstrates the potentialities of the NeQuick topside formulation when the three topside parameters are properly described.

Moreover, concerning the corresponding role played by each of the topside parameters, the main outcomes of the investigation are:

- The parameter $H_0$ is the most important one and alone succeeds in well reproducing this low-latitude behavior as a function of the altitude. This means that being able to model $H_0$ no longer as a function of the F2-layer parameters, as done by the original NeQuick model, but on the basis of COSMIC-1 data, represents a significant improvement;
- The different tests performed showed that $g$ and $r$ retrieved using COSMIC-1 data must be considered simultaneously. This is due to the limited orbit altitude of COSMIC-1 that does not allow a decoupling of $g$ and $r$ when performing a non-linear fit of the scale height. To estimate correctly $g$ and $r$ there is a need of profiles that reach much higher altitudes, where the effect of $r$ is greater than that of $g$. Unfortunately, such a kind of RO data are not currently available;
- Without solving the problem related to the parameter $r$, the simplest option to mitigate the low-latitude NeQuick mismodelling is to consider the $H_0$ values retrieved from COSMIC-1 and constant values for $g$ and $r$. However, these constant values must be different from those of the original NeQuick. This way of operating would keep intact the philosophy of the NeQuick model, which considers constant values for $g$ and $r$, with the advantage of having $H_0$ values obtained from measurements made in the topside and no longer dependent on the F2-layer and bottomside parameters.

In conclusion, the results of this study highlight how the NeQuick topside model can describe the expected latitudi-

nal and altitudinal distribution of the ionospheric electron density in the low-latitude topside ionosphere with a fine-tuned choice of the three topside parameters $H_0$, $g$, and $r$. However, for a complete description of the entire topside ionosphere, for different conditions, we need a model of the three NeQuick topside parameters $H_0$, $g$, and $r$. The procedure proposed by Pignalberi et al. (2022) and applied to COSMIC-1 RO profiles provides a reliable dataset for both $H_0$ and $g$ parameters, but does not succeed in describing the $r$ behavior at low latitudes due to the limited altitudinal range covered by COSMIC-1 satellites. This is an issue that needs to be faced in the near future by considering alternative data sources, before tackling the modelling of the three NeQuick topside parameters for an improved topside ionosphere representation.

## Declaration of Competing Interest

The authors declare that they have no known competing financial interests or personal relationships that could have appeared to influence the work reported in this paper.

## Acknowledgements

The IRI team is acknowledged for developing and maintaining the IRI model and for giving access to the corresponding Fortran code via the IRI Web site (http://irimodel.org/). The authors thank the Telecommunications/ICT for Development (T/ICT4D) Laboratory Team, The Abdus Salam International Centre for Theoretical Physics, Trieste, Italy, for developing, maintaining, and making available the NeQuick model (https://t-ict4d.ictp.it/nequick2/nequick-2-web-model). Thanks are due to the COSMIC/FORMOSAT-3 team for making freely available radio occultation data by means of the COSMIC Data Analysis and Archive Center (CDAAC, http://cdaac-www.cosmic.ucar.edu/cdaac/products.html). CHAMP data were downloaded from ftp://isdcftp.gfz-potsdam.de/champ/ME/Level2/PLPT/, Swarm A and B data from ftp://swarm-diss.eo.esa.int/Level1b/Latest_baselines/EFIx_LP/, ICON data from ftp://icon-science.ssl.berkeley.edu/pub/LEVEL.2/IVM-A, and DMSP F15 data from the CEDAR Madrigal database at http://cedar.openmadrigal.org/. We thank the GFZ German Research Centre for Geosciences, ESA, NASA, and NOAA for making freely available LEO satellites data.

The work was partially supported by the Italian MIUR-PRIN Grant 2017APKP7T on Circumterrestrial Environment: Impact of Sun–Earth Interaction.

## References

Anthes, R., Bernhardt, P.A., Chen, Y., Cucurull, L., Dymond, K.F., Ector, D., Healy, S.B., Ho, S.-P., Hunt, D.C., Kuo, Y.-H., Liu, H., Manning, K., McCormick, C., Meehan, T.K., Randel, W.J., Rocken, C., Schreiner, W.S., Sokolovskiy, S.V., Syndergaard, S., Thompson, D.C., Trenberth, K.E., Wee, T.-K., Yen, N.L., Zeng, Z., 2008. The COSMIC/FORMOSAT-3 mission: early results. Bull. Amer. Meteorol. Soc. 89, 313–333. https://doi.org/10.1175/BAMS-89-3-313.

Bilitza, D., 2004. A correction for the IRI topside electron density model based on Alouette/ISIS topside sounder data. Adv. Space Res. 33 (6), 838–843. https://doi.org/10.1016/j.asr.2003.07.009.

Bilitza, D., 2009. Evaluation of the IRI-2007 model options for the topside electron density. Adv. Space Res. 44 (6), 701–706. https://doi.org/10.1016/j.asr.2009.04.036.

Bilitza, D., Reinisch, B.W., Radicella, S.M., Pulinets, S., Gulyaeva, T., Triskova, L., 2006. Improvements of the International Reference Ionosphere model for the topside electron density profile. Radio Sci. 41, RS5S15. https://doi.org/10.1029/2005RS003370.

Bilitza, D., Pezzopane, M., Truhlik, V., Altadill, D., Reinisch, B.W., Pignalberi, A., 2022. The International Reference Ionosphere model: A review and description of an ionospheric benchmark e2022RG000792. Rev. Geophys. 60. https://doi.org/10.1029/2022RG000792.

Bilitza, D., Xiong, C., 2021. A solar activity correction term for the IRI topside electron density model. Adv. Space Res. 68 (5), 2124–2137. https://doi.org/10.1016/j.asr.2020.11.012.

Bilitza, D., 1990. International Reference Ionosphere 1990. National Space Science Data Center, Report 90-22. https://irimodel.org/docs/IRI1990pp0-84.pdf.

Catapano, F., Buchert, S., Qamili, E., Nilsson, T., Bouffard, J., Siemes, C., Coco, I., D'Amicis, R., Tøffner-Clausen, L., Trenchi, L., et al., 2022. Swarm Langmuir probes' data quality validation and future improvements. Geosci. Instrum. Methods Data Syst. 11, 149–162. https://doi.org/10.5194/gi-11-149-2022.

Chapman, S., 1931. The absorption and dissociative or ionizing effect of monochromatic radiation in an atmosphere on a rotating Earth. Proc. Phys. Soc. London 43 (1), 26–45.

Clette, F., Lefèvre, L., 2016. The new sunspot number: assembling all corrections. Sol. Phys. 291, 2629–2651. https://doi.org/10.1007/s11207-016-1014-y.

Clette, F., Svalgaard, L., Vaquero, J.M., et al., 2014. Revisiting the Sunspot Number. Space Sci. Rev. 186, 35–103. https://doi.org/10.1007/s11214-014-0074-2.

Cliver, E.W., 2016. Comparison of new and old sunspot number time series. Sol. Phys. 291, 2891–2916. https://doi.org/10.1007/s11207-016-0929-7.

Coïsson, P., Radicella, S.M., Leitinger, R., Nava, B., 2006. Topside electron density in IRI and NeQuick: features and limitations. Adv. Space Res. 37 (5), 937–942. https://doi.org/10.1016/j.asr.2005.09.015.

Coïsson, P., Nava, B., Radicella, S.M., 2009. On the use of NeQuick topside option in IRI-2007. Adv. Space Res. 43 (11), 1688–1693. https://doi.org/10.1016/j.asr.2008.10.035.

Coïsson, P., Radicella, S.M., 2005. Ionospheric topside models compared with experimental electron density profiles. Ann. Geophys.-IT 48 (3). https://doi.org/10.4401/ag-3214.

Fonda, C., Coïsson, P., Nava, B., Radicella, S.M., 2005. Comparison of analytical functions used to describe topside electron density profiles with satellite data. Ann. Geophys. 48 (3). https://doi.org/10.4401/ag-3213.

Friis-Christensen, E., Lühr, H., Hulot, G., 2006. Swarm: A constellation to study the Earth's magnetic field. Earth, Planets Space 58, 351–358. https://doi.org/10.1186/BF03351933.

Friis-Christensen, E., Lühr, H., Knudsen, D., Haagmans, R., 2008. Swarm – An Earth Observation Mission investigating Geospace. Adv. Space Res. 41, 210–216. https://doi.org/10.1016/j.asr.2006.10.008.

Garner, T.W., Taylor, B.T., Gaussiran, T.L., Coley, W.R., Hairston, M. R., Rich, F.J., 2010. Statistical behavior of the topside electron density as determined from DMSP observations: a probabilistic climatology. J. Geophys. Res. 115, A07306. https://doi.org/10.1029/2009JA014695.

Habarulema, J.B., Okoh, D., Bergeot, N., Burešová, D., Matamba, T., Tshisaphungo, M., Katamzi-Joseph, Z., Pinat, E., Chevalier, J.-M., Seemala, G., 2021. Interhemispheric comparison of the ionosphere and plasmasphere total electron content using GPS, radio occultation and ionosonde observations. Adv. Space Res. 68 (6), 2339–2353. https://doi.org/10.1016/j.asr.2021.05.004.

He, J., Yue, X., Le, H., Ren, Z., Ding, F., 2022. High-resolution and accurate low-latitude gridded electron density generation and evaluation e2021JA030192. J. Geophys. Res. Space Phys. 127. https://doi.org/10.1029/2021JA030192.

Heelis, R.A., Stoneback, R.A., Perdue, M.D., et al., 2017. Ion velocity measurements for the ionospheric connections explorer. Space Sci. Rev. 212, 615–629. https://doi.org/10.1007/s11214-017-0383-3.

Hoque, M.M., Jakowski, N., 2012. Ionospheric propagation effects on GNSS signals and new correction approaches. In: Jin, S. (Ed.) Global Navigation Satellite Systems, IntechOpen, Rijeka, pp. 381–405. https://doi.org/10.5772/30090 (Chapter 16).

Hunsucker, R.D., 1991. Radio Techniques for Probing the Terrestrial Ionosphere. Springer, Berlin, Heidelberg. https://doi.org/10.1007/978-3-642-76257-4.

Immel, T.J., England, S.L., Mende, S.B., et al., 2018. The ionospheric connection explorer mission: mission goals and design. Space Sci. Rev. 214, 13. https://doi.org/10.1007/s11214-017-0449-2.

Kashcheyev, A., Nava, B., 2019. Validation of NeQuick 2 model topside ionosphere and plasmasphere electron content using COSMIC POD TEC. J. Geophys. Res. Space Physics 124, 9525–9536. https://doi.org/10.1029/2019JA026971.

Knudsen, D.J., Burchill, J.K., Buchert, S.C., Eriksson, A.I., Gill, R., Wahlund, J.-E., Åhlen, L., Smith, M., Moffat, B., 2017. Thermal ion imagers and Langmuir probes in the Swarm electric field instruments. J. Geophys. Res. Space Physics 122, 2655–2673. https://doi.org/10.1002/2016JA022571.

Leitinger, R., Nava, B., Hochegger, G., Radicella, S., 2001. Ionospheric profilers using data grids. Phys. Chem. Earth – Part C: Solar, Terr. Plan. Science 26 (5), 293–301. https://doi.org/10.1016/S1464-1917(01)00002-2.

Leitinger, R., Radicella, S., Hochegger, G., Nava, B., 2002. Diffusive equilibrium models for the height region above the F2 peak. Adv. Space Res. 29 (6), 809–814. https://doi.org/10.1016/S0273-1177(02)00036-4.

Leitinger, R., Zhang, M.L., Radicella, S.M., 2005. An improved bottomside for the ionospheric electron density model NeQuick. Ann. Geophys.-IT 48 (3). https://doi.org/10.4401/ag-3217.

Mosert de Gonzales, M., Radicella, S.M., 1990. On a characteristic point at the base of F2 layer in the ionosphere. Adv. Space Res. 10 (11), 17–25. https://doi.org/10.1016/0273-1177(90)90300-O.

Nava, B., Radicella, S.M., Pulinets, S., Depuev, V., 2001. Modelling bottom and topside electron density and TEC with profile data from topside ionograms. Adv. Space Res. 27 (1), 31–34. https://doi.org/10.1016/S0273-1177(00)00137-X.

Nava, B., Coïsson, P., Radicella, S.M., 2008. A new version of the NeQuick ionosphere electron density model. J. Atmos. Solar-Terr. Phys. 70 (15), 1856–1862. https://doi.org/10.1016/j.jastp.2008.01.015.

Nsumei, P., Reinisch, B.W., Huang, X., Bilitza, D., 2012. New Vary-Chap profile of the topside ionosphere electron density distribution for use with the IRI model and the GIRO real time data. Radio Sci. 47, RS0L16. https://doi.org/10.1029/2012RS004989.

Olivares-Pulido, G., Hernández-Pajares, M., Aragón-Àngel, A., Garcia-Rigo, A., 2016. A linear scale height chapman model supported by GNSS occultation measurements. J. Geophys. Res. Space Phys. 121, 7932–7940. https://doi.org/10.1002/2016JA022337.

Park, J., 2022. Ratio between oversatellite electron content and plasma density measured by Swarm: a proxy for topside scale height e2021JA030137. J. Geophys. Res. Space Phys. 127. https://doi.org/10.1029/2021JA030137.

Pezzopane, M., Pignalberi, A., 2019. The ESA Swarm mission to help ionospheric modeling: A new NeQuick topside formulation for mid-latitude regions. Sci. Rep. 9 (1), 12253. https://doi.org/10.1038/s41598-019-48440-6.

Pignalberi, A., Pezzopane, M., Tozzi, R., De Michelis, P., Coco, I., 2016. Comparison between IRI and preliminar Swarm Langmuir probe measurements during the St. Patrick storm period. Earth, Planets Space 68 (1), 93. https://doi.org/10.1186/s40623-016-0466-5.

Pignalberi, A., Pezzopane, M., Rizzi, R., 2018a. Modeling the lower part of the topside ionospheric vertical electron density profile over the European region by means of Swarm satellites data and IRI UP method. Space Weather 16. https://doi.org/10.1002/2017SW001790.

Pignalberi, A., Pezzopane, M., Rizzi, R., Galkin, I., 2018b. Effective solar indices for ionospheric modeling: a review and a proposal for a real-time regional IRI. Surv. Geophys. 39, 125–167. https://doi.org/10.1007/s10712-017-9438-y.

Pignalberi, A., Pietrella, M., Pezzopane, M., Rizzi, R., 2018c. Improvements and validation of the IRI UP method under moderate, strong, and severe geomagnetic storms. Earth, Planets Space 70, 180. https://doi.org/10.1186/s40623-018-0952-z.

Pignalberi, A., Pezzopane, M., Themens, D.R., Haralambous, H., Nava, B., Coïsson, P., 2020a. On the analytical description of the topside ionosphere by NeQuick: Modeling the scale height through COSMIC/FORMOSAT-3 selected data. IEEE J. Sel. Topics Appl. Earth Observ. Remote Sens. 13, 1867–1878. https://doi.org/10.1109/JSTARS.2020.2986683.

Pignalberi, A., Pezzopane, M., Nava, B., Coïsson, P., 2020b. On the link between the topside ionospheric effective scale height and the plasma ambipolar diffusion, theory and preliminary results. Sci. Rep. 10 (1), 17541. https://doi.org/10.1038/s41598-020-73886-4.

Pignalberi, A., Nava, B., Pietrella, M., Cesaroni, C., Pezzopane, M., 2021. Midlatitude climatology of the ionospheric equivalent slab thickness over two solar cycles. J. Geod. 95, 124. https://doi.org/10.1007/s00190-021-01577-7.

Pignalberi, A., Pezzopane, M., Nava, B., 2022. Optimizing the NeQuick topside scale height parameters through COSMIC/FORMOSAT-3 radio occultation data. IEEE Geosc. Rem. Sens. Lett. 19, 1–5. https://doi.org/10.1109/LGRS.2021.3096657.

Prol, F.d.S., Hernández-Pajares, M., Camargo, P.D.O., Muella, M.T.D.A.H., 2018. Spatial and temporal features of the topside ionospheric electron density by a new model based on GPS radio occultation data. J. Geophys. Res. Space. Phys. 123, 2104–2115. https://doi.org/10.1002/2017JA024936.

Prol, F.d.S., Themens, D., Hernández-Pajares, M., Camargo, P.D.O., Muella, M.T.D.A.H., 2019. Linear vary-chap topside electron density model with topside sounder and radio-occultation data. Surv. Geophys. 40, 277–293. https://doi.org/10.1007/s10712-019-09521-3.

Prol, F.d.S., Smirnov, A.G., Hoque, M.M., Shprits, Y.Y., 2022. Combined model of topside ionosphere and plasmasphere derived from radio-occultation and Van Allen Probes data. Sci. Rep. 12, 9732. https://doi.org/10.1038/s41598-022-13302-1.

Radicella, S.M., Leitinger, R., 2001. The evolution of the DGR approach to model electron density profiles. Adv. Space Res. 27 (1), 35–40. https://doi.org/10.1016/S0273-1177(00)00138-1.

Radicella, S.M., Alazo-Cuartas, K., Migoya-Orué, Y., Kashcheyev, A., 2021. Thickness parameters in the empirical modeling of bottomside electron density profiles. Adv. Space Res. 68 (5), 2069–2075. https://doi.org/10.1016/j.asr.2020.12.037.

Rawer, K., 1988. Synthesis of ionospheric electron density profiles with Epstein functions. Adv. Space Res. 8 (4), 191–199. https://doi.org/10.1016/0273-1177(88)90239-6.

Reigber, C., Lühr, H., Schwintzer, P., Wickert, J., 2004. Earth observation with CHAMP. Results from three years. Springer Berlin, Heidelberg. 10.1007/b138105.

Reinisch, B.W., Nsumei, P., Huang, X., Bilitza, D., 2007. Modeling the F2 topside and plasmasphere for IRI using IMAGE/RPI and ISIS data. Adv. Space Res. 39 (5), 731–738. https://doi.org/10.1016/j.asr.2006.05.032.

Rishbeth, H., Garriott, O., 1969. Introduction to ionospheric physics, International geophysics series, Vol. 14. Academic Press, New York.

Rother, M., Michaelis, I., 2019. CH-ME-2-PLPT - CHAMP electron density and temperature time series in low time resolution (Level 2). GFZ Data Services. https://doi.org/10.5880/GFZ.2.3.2019.007.

Singh, A.K., Haralambous, H., Oikonomou, C., 2021. Validation and improvement of NeQuick topside ionospheric formulation using

COSMIC/FORMOSAT-3 data e2020JA028720. J. Geophys. Res. Space. Phys. 126. https://doi.org/10.1029/2020JA028720.

Themens, D.R., Jayachandran, P.T., Bilitza, D., Erickson, P.J., Häggström, I., Lyashenko, M.V., Reid, B., Varney, R.H., Pustovalova, L., 2018. Topside electron density representations for middle and high latitudes: A topside parameterization for E-CHAIM based on the NeQuick. J. Geophys. Res. Space Phys. 123, 1603–1617. https://doi.org/10.1002/2017JA024817.

Vaishnav, R., Jin, Y., Golam Mostafa, M., Aziz, S.R., Zhang, S.-R., Jacobi, C., 2021. Study of the upper transition height using ISR observations and IRI predictions over Arecibo. Adv. Space Res. 68 (5), 2177–2185. https://doi.org/10.1016/j.asr.2020.10.010.

Verhulst, T., Stankov, S.M., 2014. Evaluation of ionospheric profilers using topside sounding data. Radio Sci. 49, 181–195. https://doi.org/10.1002/2013RS005263.

Yizengaw, E., Moldwin, M.B., Galvan, D., Iijima, B.A., Komjathy, A., Mannucci, A.J., 2008. Global plasmaspheric TEC and its relative contribution to GPS TEC. J. Atmos. Solar-Terr. Phys. 70 (11–12), 1541–1548. https://doi.org/10.1016/j.jastp.2008.04.022.